Cs-TEM vs Cs-STEM

Duncan Alexander
EPFL-CIME

FEI Titan Themis @ CIME EPFL

60–300 kV
Monochromator
High brightness X-FEG
Probe Cs-corrected: 0.7 Å @ 300 kV
Image Cs-corrected: 0.7 Å @ 300 kV
Super-X EDX detector
GIF Quantum ERS energy filter
Dual-channel, Ultrafast STEM-EELS
Lorentz mode
Biprism for holography
Piezo stage
Tomographic acquisition

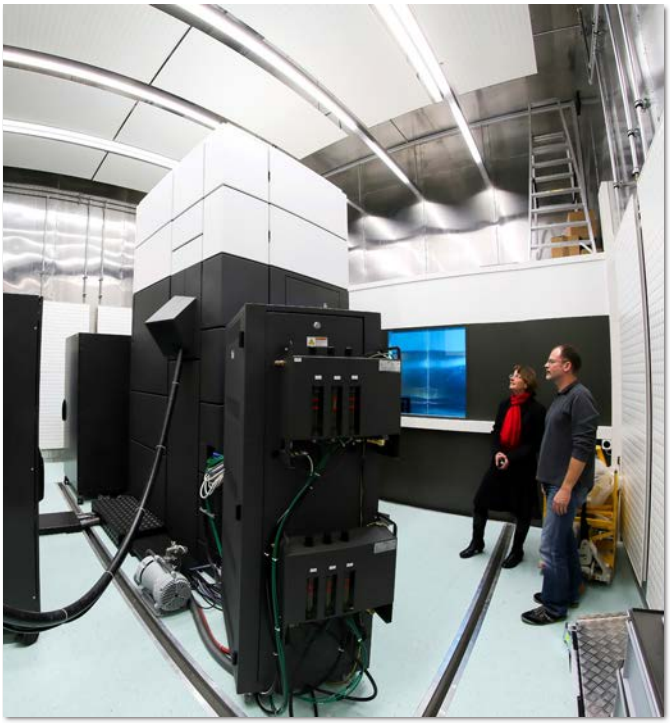

Limitation to spatial resolution: aberrations

Electromagnetic lenses in TEM column are toroidal
Lenses inherently convergent
=> spherical aberration (C_S) and chromatic aberration (C_C)

No C_S

With C_S

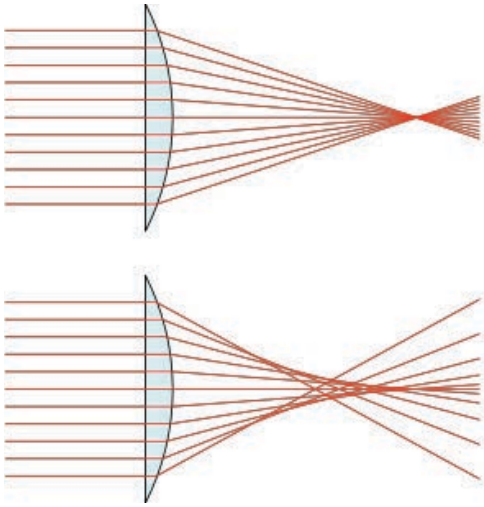

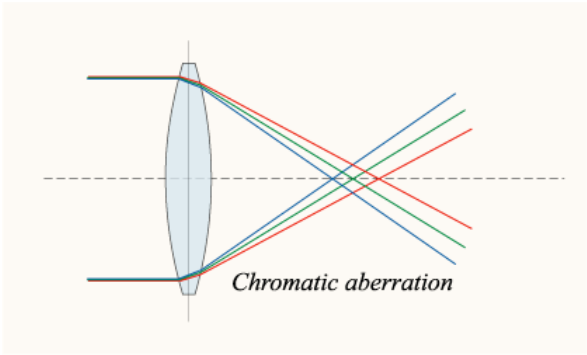

Resolution in HR-TEM limited by aberrations, especially C_S

Cs-correction (STEM and TEM)

Combination of standard radially-symmetric convergent lenses
with multipole divergent lenses (e.g. tetrapoles, hextapoles) to tune C_S

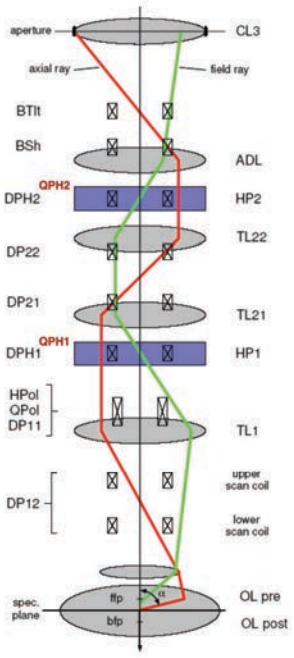

CEOS corrector

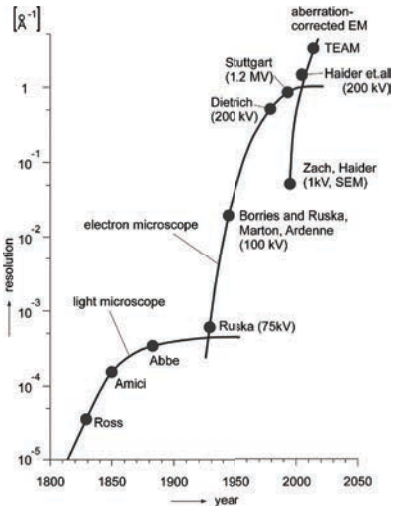

Rose J. *Electron Microscopy* **58** (2009) 77–85

Principle of aberration correction

- Compensate C_S and other distortions with equivalent but opposite components to add together with aim of giving ideal spherical wavefront

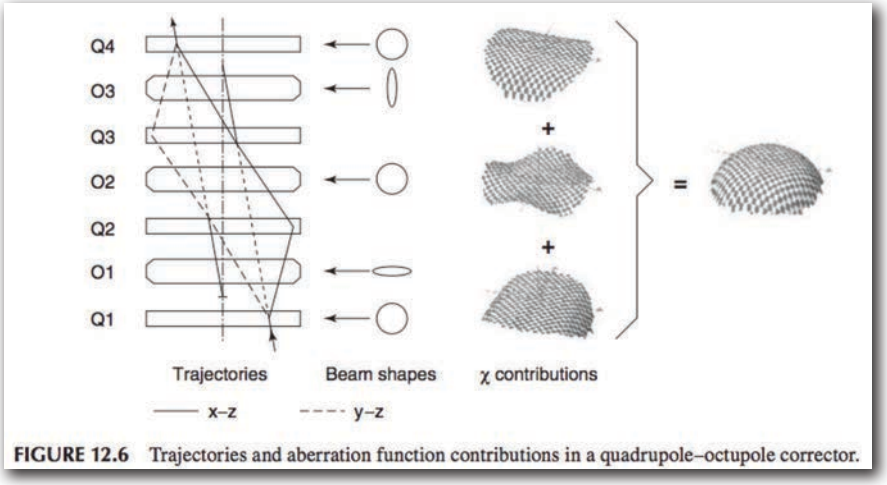

FIGURE 12.6 Trajectories and aberration function contributions in a quadrupole–octupole corrector.

Krivanek et al. Aberration Correction in Electron Microscopy, Handbook of Charged Particle Physics 2009, pp. 601–641

CEOS aberration corrector

- CEOS aberration corrector used for imaging correction in CTEM also used before sample as probe-corrector for STEM; sextapole-round lens-sextapole design. This is an "indirect" corrector type; ~30 power supplies but higher power and water cooling needed.

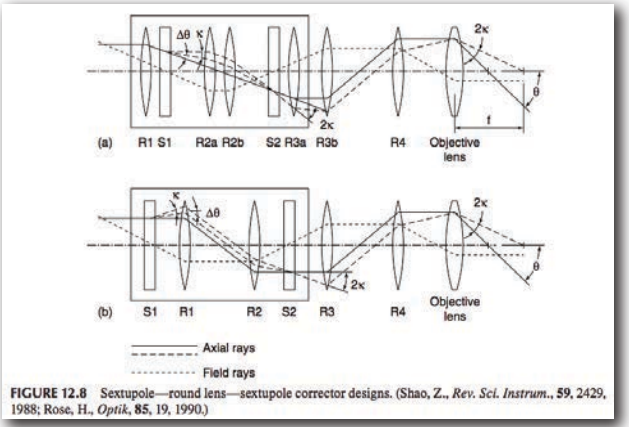

FIGURE 12.8 Sextupole—round lens—sextupole corrector designs. (Shao, Z., *Rev. Sci. Instrum.*, **59**, 2429, 1988; Rose, H., *Optik*, **85**, 19, 1990.)

Indirect-action correctors, in which the aberration to be corrected is acted on by a combination aberration arising as a by-product of a lower-order aberration intentionally created in the corrector. The undesirable lower-order aberration coefficients are typically of the same order of magnitude as the coefficients of the aberrations to be corrected. For the small angles used in electron microscopy, this means that the effect of the lower-order aberrations on the beam are very strong. These aberrations, therefore, need to be canceled very precisely, typically by using an equivalent optical element that cancels the undesirable low-order effect while at the same time increasing the desirable higher-order effect.

Krivanek et al. Aberration Correction in Electron Microscopy, Handbook of Charged Particle Physics 2009, pp. 601–641

Nion aberration corrector

- First STEM aberration corrector installed on VG by Nion (Krivanek); quadrupole-octopole design. This is a "direct-action" corrector type as now used on Nion UltraSTEM: ~70 power supplies needed but low power and which can fit onto printed circuit boards

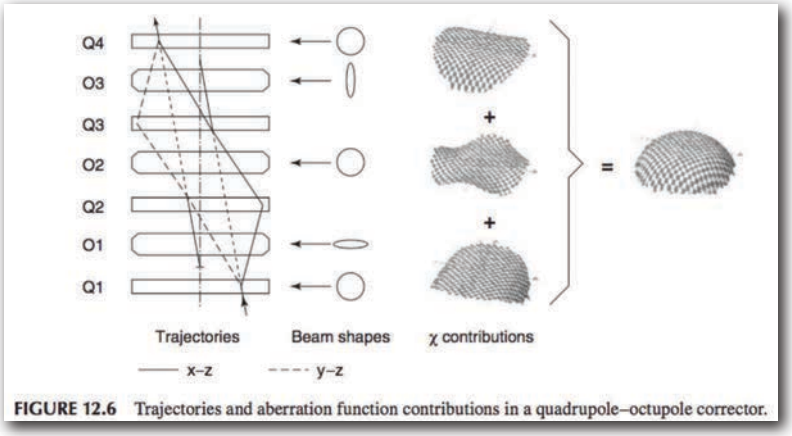

FIGURE 12.6 Trajectories and aberration function contributions in a quadrupole–octupole corrector.

Direct-action correctors, in which the principal aberration is corrected by a correcting element whose main effect is producing aberrations of the needed order. In these systems, undesirable by-product aberrations tend to arise that are of the same order and of similar magnitude as the aberrations being corrected. The by-product aberrations are typically canceled by creating different beam shapes in different stages of the apparatus, which permits the same type of optical element to produce different mixtures of aberration terms.

Krivanek et al. Aberration Correction in Electron Microscopy, Handbook of Charged Particle Physics 2009, pp. 601–641

Current correctors

- CEOS: C_S-corrected, "C_5 optimised": CETCOR, CESCOR, D-COR
- CEOS: C_S-C_C corrected (NCEM TEAM 1.0, Julich Titan Pico)
- CEOS: B-COR aplanatic optimised for far off-axis rays
- JEOL: unique C_S-C_C corrector (CCC project)
- JEOL: Dodecapole Cs corrector ("Grand ARM")
- Nion: C_S-C_5 corrected

Understanding resolution in EM

- For C_S-TEM need to understand concepts of:
  - Contrast transfer function (CTF)
  - How to use CS to optimise CTF
  - Difference between point resolution and information limit
  - Properties of the camera (MTF), sample drift, "Stobbs factor"…
- For C_S-STEM need to understand concepts of:
  - Probe size, shape, brightness, depth of field (DOF)
  - Optical transfer function (OTF); STEM first to achieve 0.5 Å res
  - Scan (in)stabilities, detectors

Cs-corrected HR-TEM "interferometry"

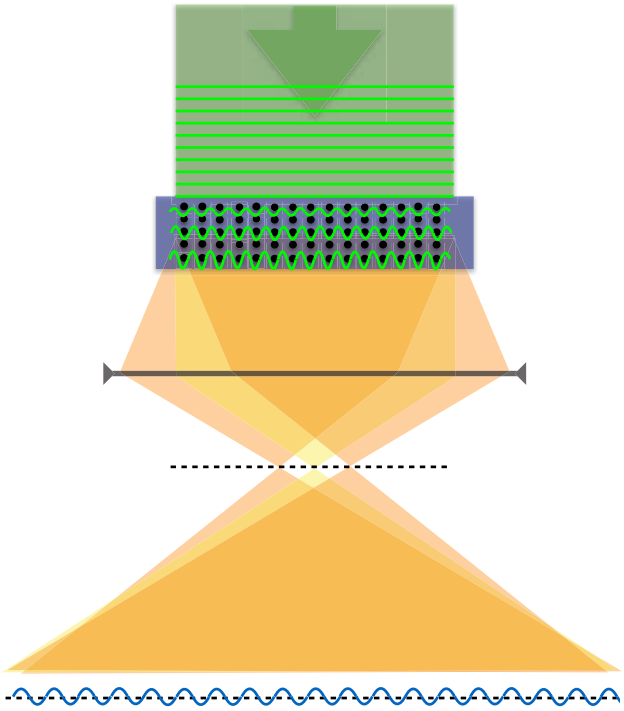

Image of "projected potential"

Example: Σ3 grain boundaries in Al

Uncorrected

C_S-corrected

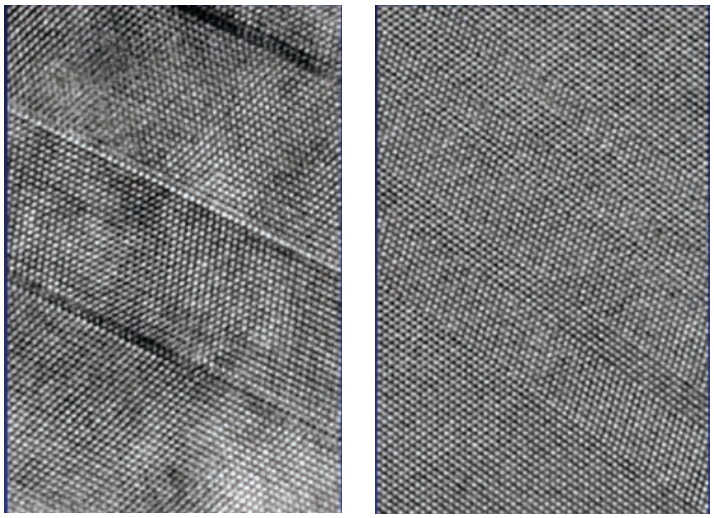

Images: Oikawa, JEOL

Reduced delocalisation in *phase contrast* image

CTF curves: uncorrected microscopes

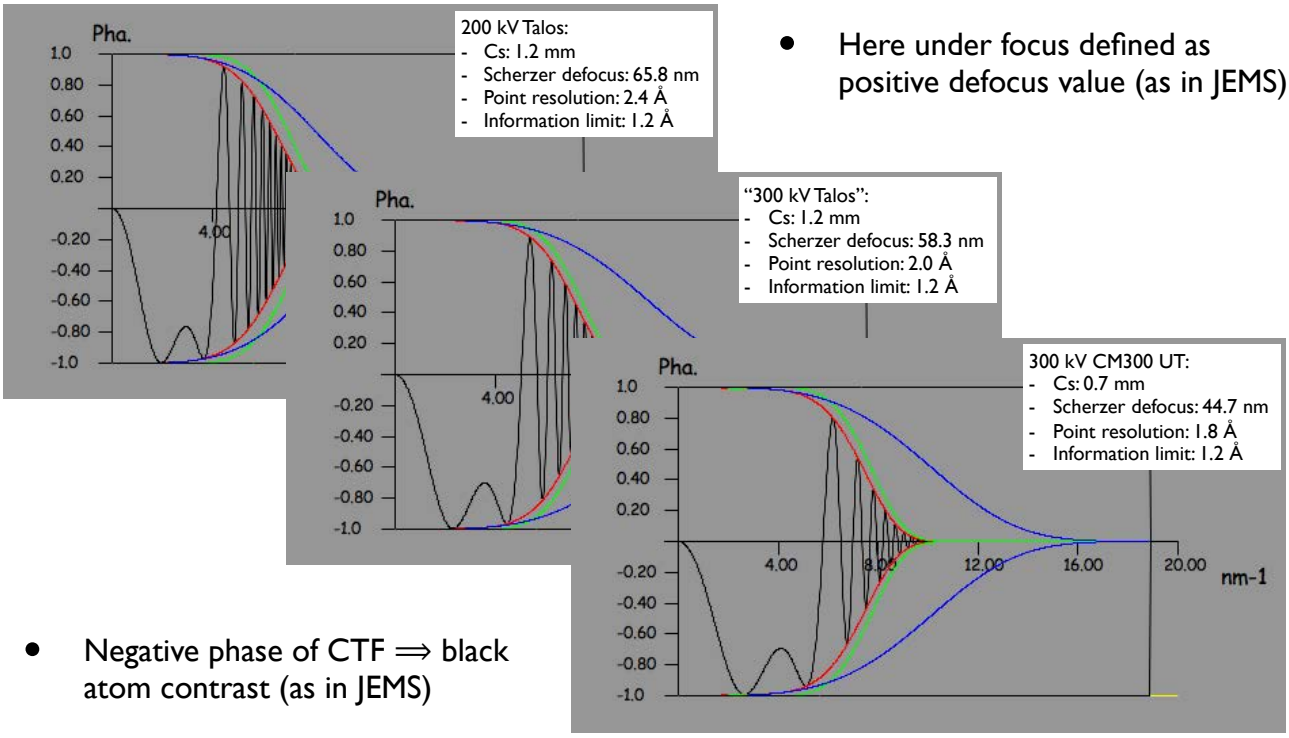

- Here under focus defined as positive defocus value (as in JEMS)

- Negative phase of CTF ⟹ black atom contrast (as in JEMS)

Cs-TEM: effect on CTF

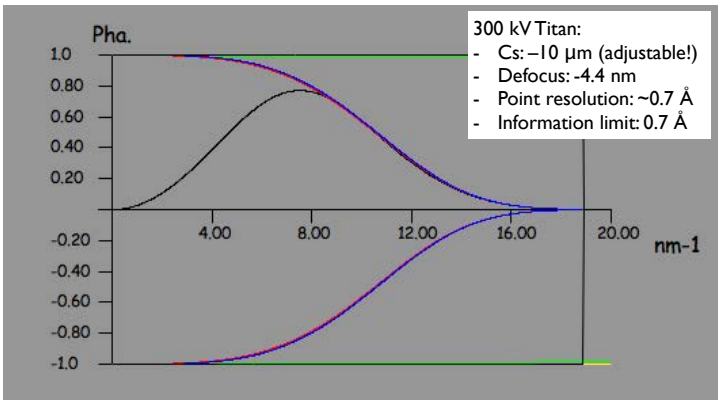

- Higher information limit from shifting spatial and temporal envelopes
- Done by improved stability of instrument + monochromatic beam
- Here show negative Cs ("white atom" contrast)
- Adjust Cs, defocus to give one wide CTF pass band to information limit

Cs-TEM example: $(Al_xGa_{1-x})As$ nanowire

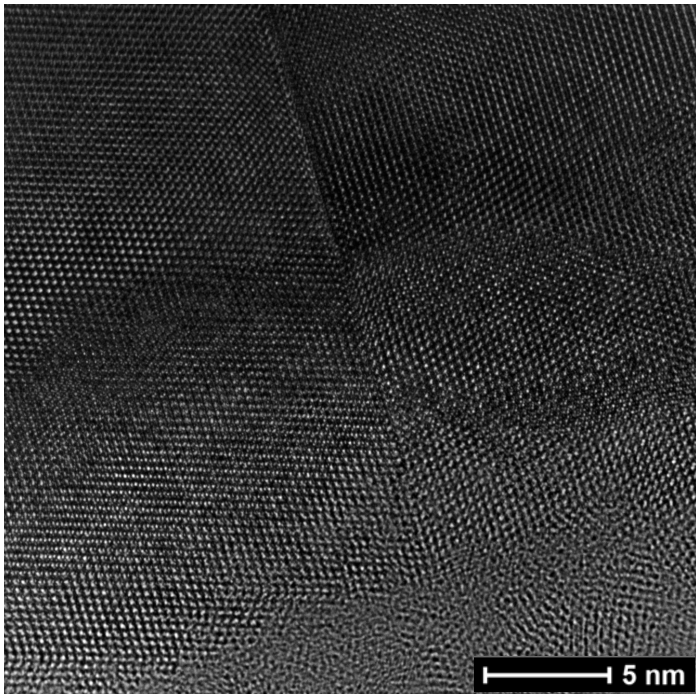

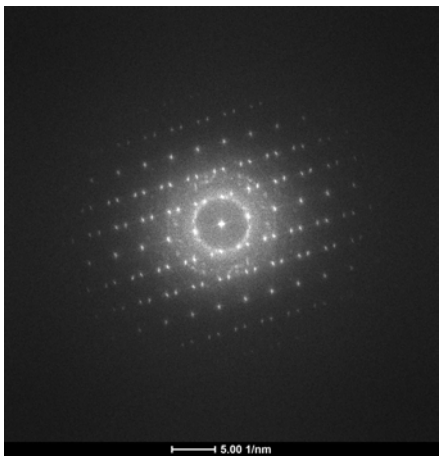

Sample courtesy of Yannick Fontana, Anna Fontcuberta-i-Morral, LMSC

Cs-TEM example: $(Al_xGa_{1-x})As$ nanowire

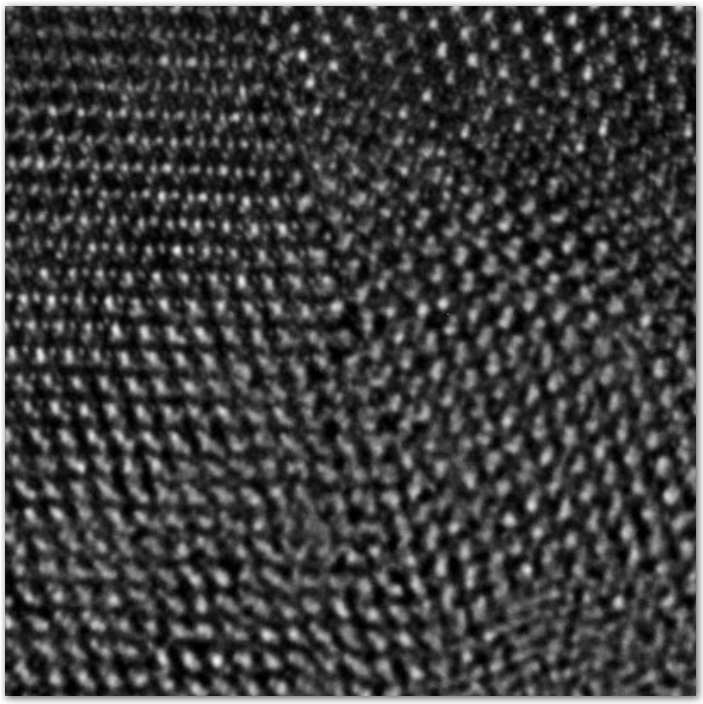

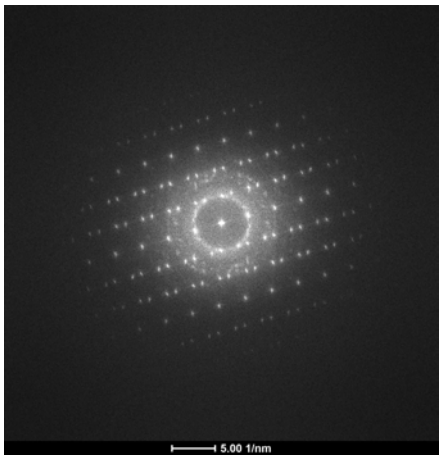

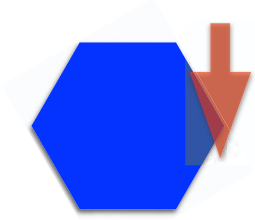

Sample courtesy of Yannick Fontana, Anna Fontcuberta-i-Morral, LMSC

Cs-TEM [1 1 0] GaAs simulation

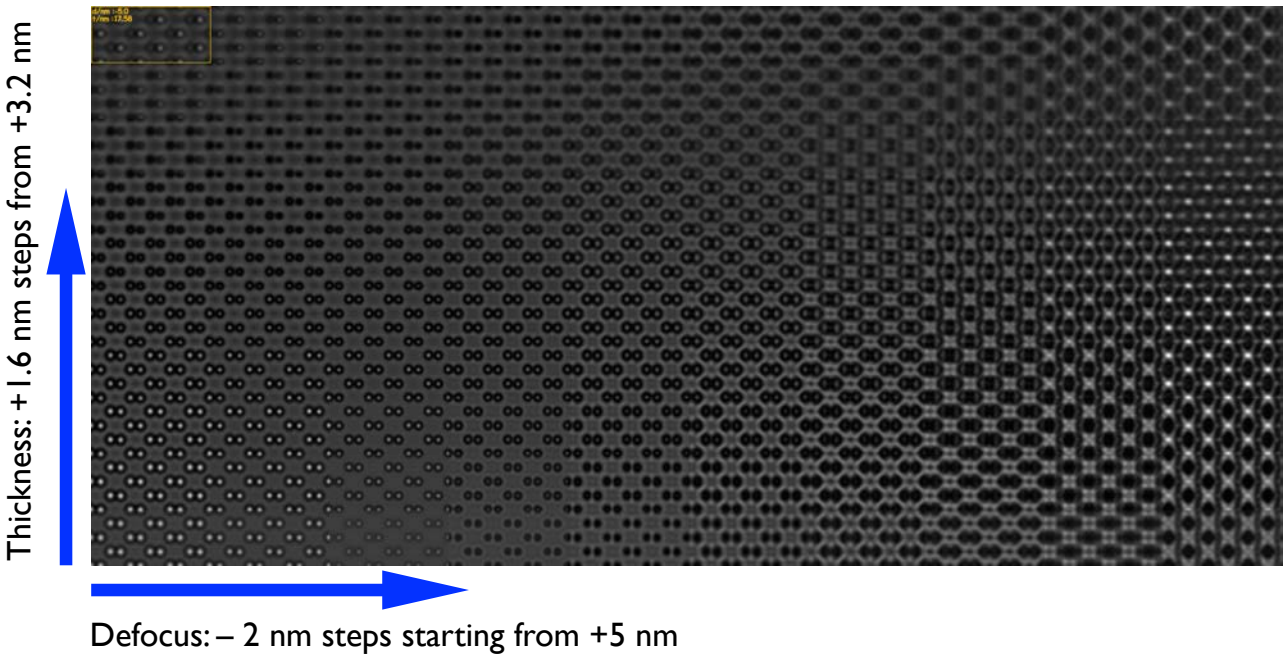

Cs-TEM: defocus effect on CTF

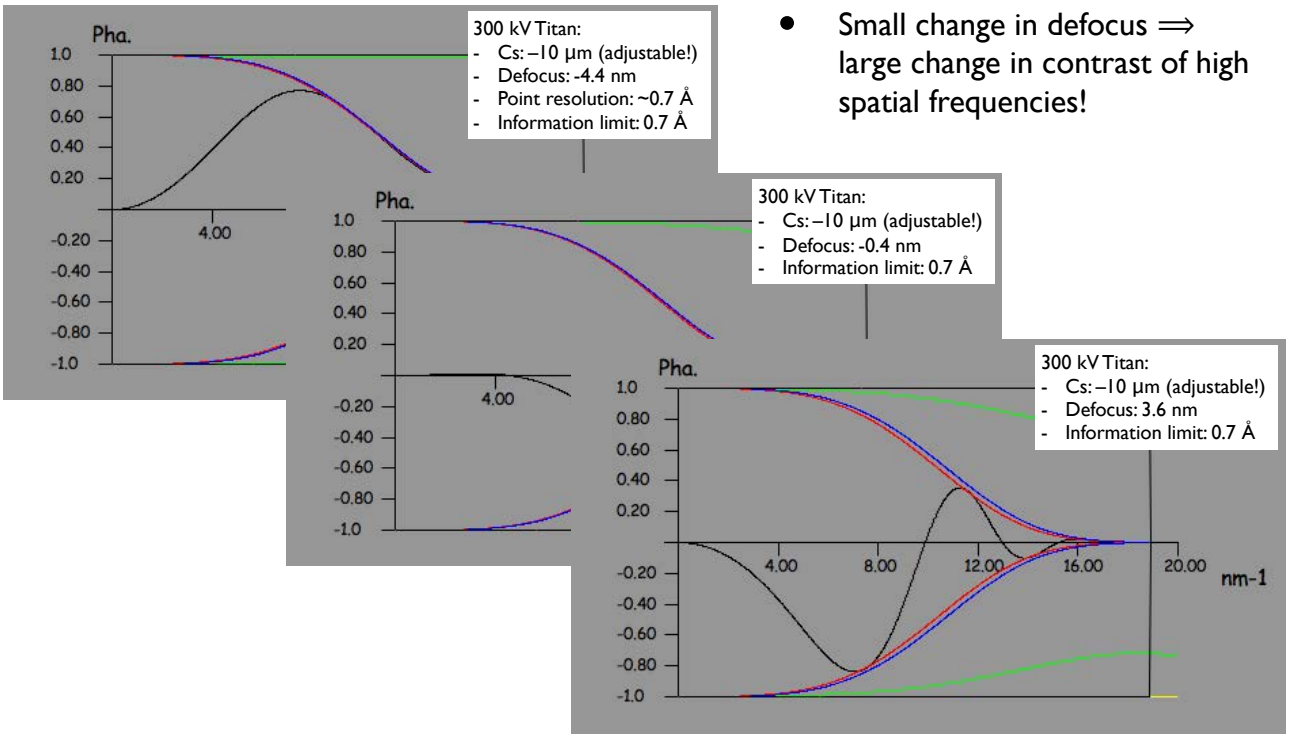

- Small change in defocus ⟹ large change in contrast of high spatial frequencies!

Cs-STEM example: $(Al_xGa_{1-x})As$ nanowire

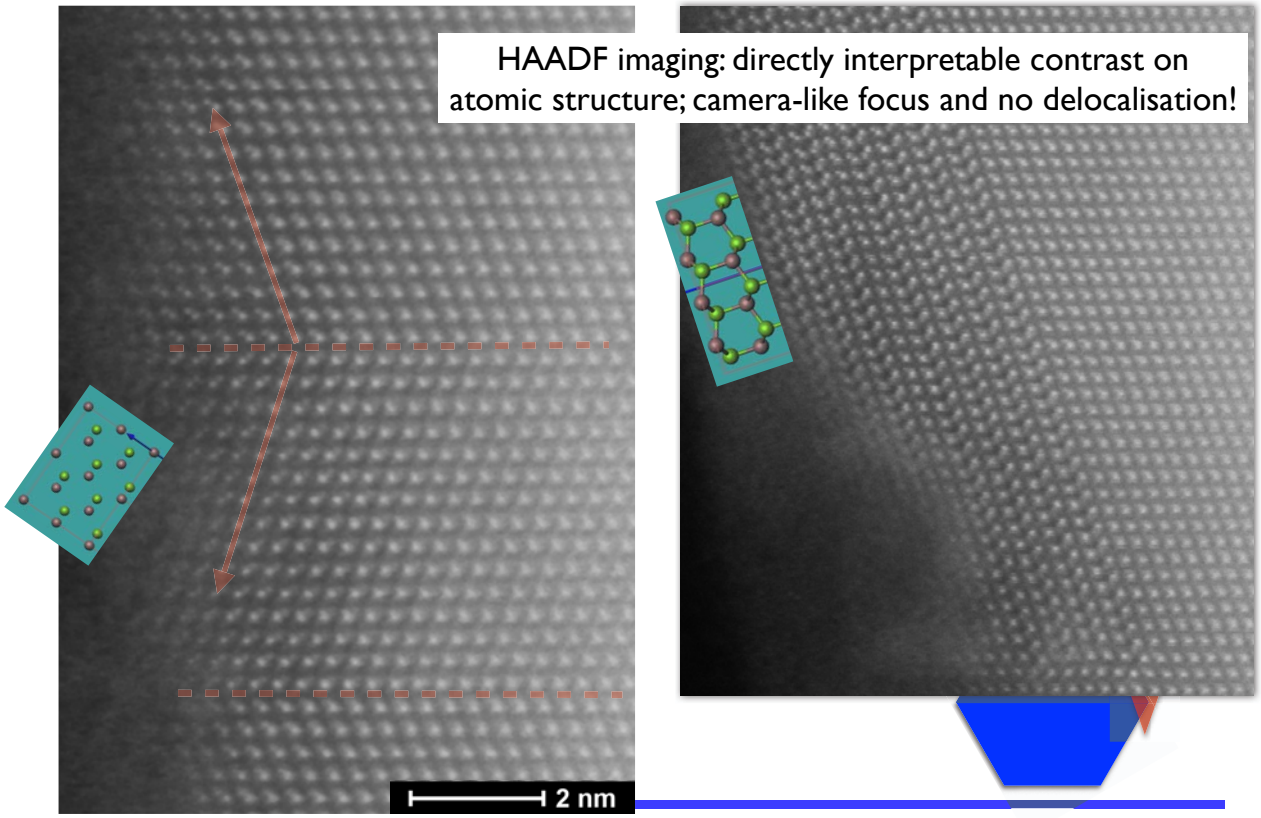

Benefits of aberration correction

Analytics – STEM-EELS

Atomic resolution core-loss STEM-EELS mapping (Nion UltraSTEM)

Atomic-Scale Chemical Imaging of Composition and Bonding by Aberration-Corrected Microscopy
D. A. Muller, *et al.*
Science **319**, 1073 (2008);
DOI: 10.1126/science.1148820

Fig. 1. Spectroscopic imaging of a $La_{0.7}Sr_{0.3}MnO_3/SrTiO_3$ multilayer, showing the different chemical sublattices in a 64 × 64 pixel spectrum image extracted from 650 eV–wide electron energy-loss spectra recorded at each pixel. **(A)** La M edge; **(B)** Ti L edge; **(C)** Mn L edge; **(D)** red-green-blue false-color image obtained by combining the rescaled Mn, La, and Ti images. Each of the primary color maps is rescaled to include all data points within two standard deviations of the image mean. Note the lines of purple at the interface in (D), which indicate Mn-Ti intermixing on the B-site sublattice. The white circles indicate the position of the La columns, showing that the Mn lattice is offset. Live acquisition time for the 64 × 64 spectrum image was ~30 s; field of view, 3.1 nm.

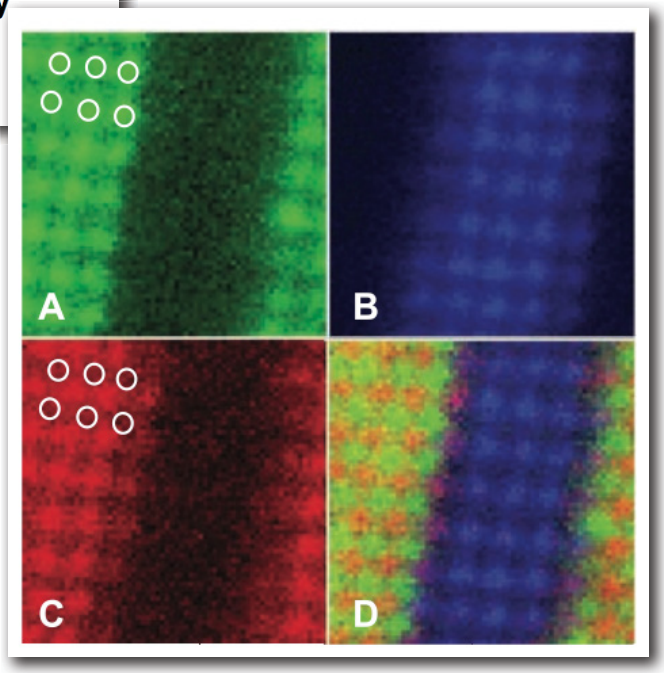

More recently: atomic resolution EDX, EFTEM – but are they as interpretable?

Measurement precision – C_S-TEM

Is science prepared for atomic-resolution electron microscopy?

Knut W. Urban

The efforts of microscopists have given aberration-corrected transmission electron microscopy the power to reveal atomic structures with unprecedented precision. It is now up to materials scientists to use this power for extracting physical properties from microscopic atomic arrangements.

An investigation using Gaussian regression analyses[11] revealed that such position measurements can be carried out at a precision of better than ±5 pm (at a 95% confidence level). Such a precision is far superior to that of any other microscopic technique, including the scanning transmission electron microscope or even the scanning tunnelling microscope. The standard objection to such extremely high precision is that it cannot be allowed by a microscope with a 70-pm Rayleigh or point resolution[19,20]. However, resolution and precision are two separate physical terms. Although resolution is defined by the minimum separation of two optically broadened intensity peaks at which these can just be separated in the image, the distance between two well-isolated peaks, fitted for example by two-dimensional Gaussians, can be measured at a precision more than an order of magnitude higher.

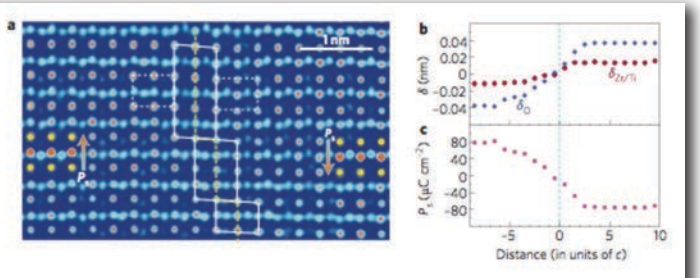

Figure 2 | Polarization domain wall in ferroelectric PZT. **a**, Atomic structure. Arrows give the direction of the spontaneous polarization, which can be directly inferred from the local atom displacements. The shifts of the oxygen atoms (blue circles) out of the Ti/Zr-atom rows (red circles) can be seen directly, as can the change in separation between Ti/Zr and Pb (yellow circles). **b**, Atomic-resolution measurements of the shifts of oxygen (δ_O), and titanium/zirconium ($\delta_{Ti/Zr}$) atoms as a function of distance from the wall centre (units of *c*-lattice parameter) in a longitudinal-inversion domain wall; **c**, The value of the local polarization P_s that can be calculated from these data. Adapted from ref. 12. © 2008 NPG.

260

NATURE MATERIALS | VOL 8 | APRIL 2009 |

Measurement precision – C_S-STEM

Mapping Octahedral Tilts and Polarization Across a Domain Wall in $BiFeO_3$ from Z-Contrast Scanning Transmission Electron Microscopy Image Atomic Column Shape Analysis

Albina Y. Borisevich,[†,*] Oleg S. Ovchinnikov,[‡] Hye Jung Chang,[†] Mark P. Oxley,[†,§] Pu Yu,[⊥] Jan Seidel,[⊥] Eugine A. Eliseev,[∥] Anna N. Morozovska,[#] Ramamoorthy Ramesh,[⊥] Stephen J. Pennycook,[†] and Sergei V. Kalinin[†]

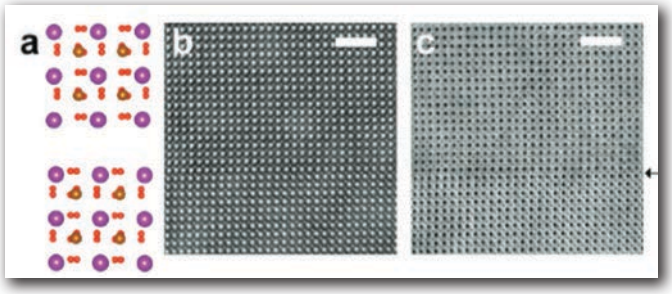

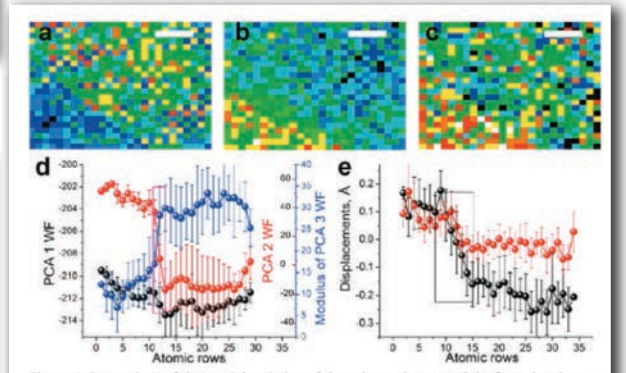

Figure 6. Comparison of the spatial variation of the column shapes and the ferroelectric polarization across the domain wall: (a) absolute value of the third PCA weight factor map (see Figure 4h). (b and c) Polarization maps for out-of-plane (b) and in-plane (c) polarization based on the Bi and Fe column displacements measured from the Z-contrast image. (d) Profiles of different PCA weight factor maps across the domain wall: first (black) (see Figure 4f), second (red) (see Figure 4g), and the absolute value of the third component (blue) (see Figure 6a); note the atomically sharp transition in the second and third PCA weight factor map profiles. (e) Profiles of out-of-plane (black) and in-plane (red) polarization maps (see b and c) across the domain wall showing a diffuse transition. Scale bars are 2 nm.

VOL. 4 ▪ NO. 10 ▪ 6071–6079 ▪ 2010 ACSNANO

Measurement precision – C_S-STEM

- Analysis of $LaVO_3$ film grown under epitaxial strain on $DyScO_3$ substrate

HAADF ABF (inverted contrast)

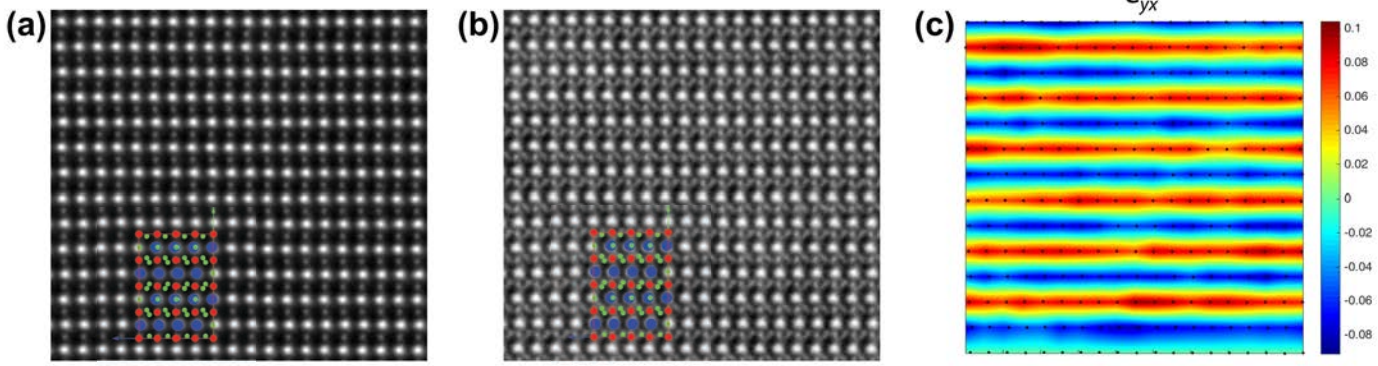

- Simultaneously acquired HAADF and ABF scan image series
- HAADF series corrected for linear and non-linear scan distortions to produce aligned and averaged image; alignments applied to ABF series also
- HAADF shows anti-ferroelectric charge ordering of La cations; ABF also shows projected rotations of O anion octahedra

Meley et al. APL Materials **6** (2018) 046102

The move to lower kV

- Before C_S-correction highest resolution by minimising λ (MeV instruments with λ < 1 pm)
- Light materials (graphene, nanotubes, …) suffer knock-on damage. Some thresholds:
  - Bulk graphene: 86 keV
  - Graphene edge atom: 36 keV
- Therefore need low kV – 80 kV max but 60 kV better – which have long wavelengths
- Aberration correction now mandatory for atomic resolution
- Notable projects: Suenaga CCC project (30 kV aim), Ute Kaiser's Salve project (20 kV aim), both with combined C_S-C_C correctors; new UltraSTEM (20 – 100 kV range)

Imaging organic molecules – Cs-(S)TEM

Cs-TEM (80 keV beam): imaging of molecule as weak phase object

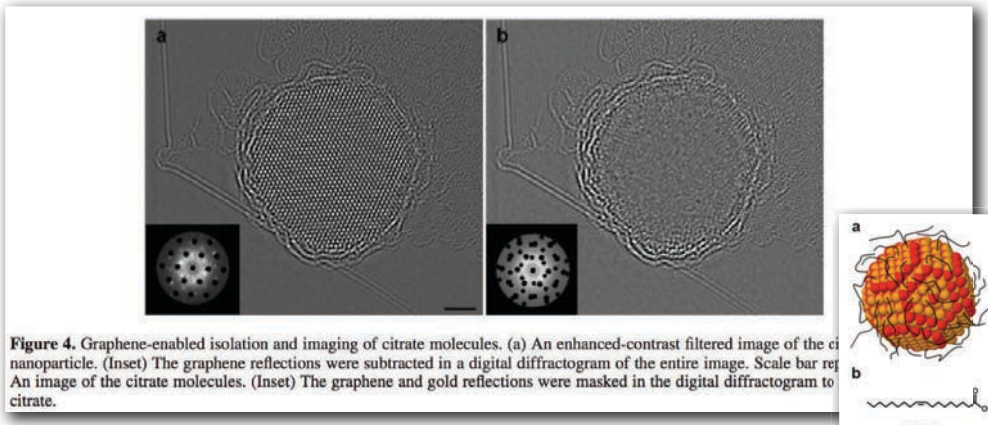

Figure 4. Graphene-enabled isolation and imaging of citrate molecules. (a) An enhanced-contrast filtered image of the ci nanoparticle. (Inset) The graphene reflections were subtracted in a digital diffractogram of the entire image. Scale bar re An image of the citrate molecules. (Inset) The graphene and gold reflections were masked in the digital diffractogram to citrate.

Lee et al. Nano Letters 9 (2009) 3365–3369

Cs-STEM (200 keV beam):
imaging of molecules by HAADF;
need very clean (un-contaminating) sample

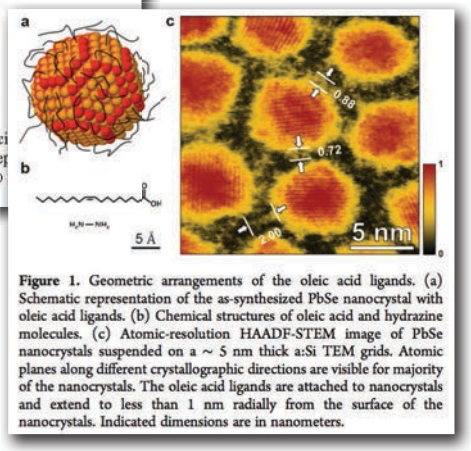

Figure 1. Geometric arrangements of the oleic acid ligands. (a) Schematic representation of the as-synthesized PbSe nanocrystal with oleic acid ligands. (b) Chemical structures of oleic acid and hydrazine molecules. (c) Atomic-resolution HAADF-STEM image of PbSe nanocrystals suspended on a ~ 5 nm thick a:Si TEM grids. Atomic planes along different crystallographic directions are visible for majority of the nanocrystals. The oleic acid ligands are attached to nanocrystals and extend to less than 1 nm radially from the surface of the nanocrystals. Indicated dimensions are in nanometers.

Gunawan et al. Chem. Mater 26 (2014) 3328–3333

Imaging organic molecules – Cs-TEM

- Iron oxide nanoparticles functionalised with folic acid
- Aberration-corrected phase contrast imaging at 80 keV using Titan Themis at CIME
- Incident electron beam monochromated to improve temporal coherence/reduce effect of chromatic aberration

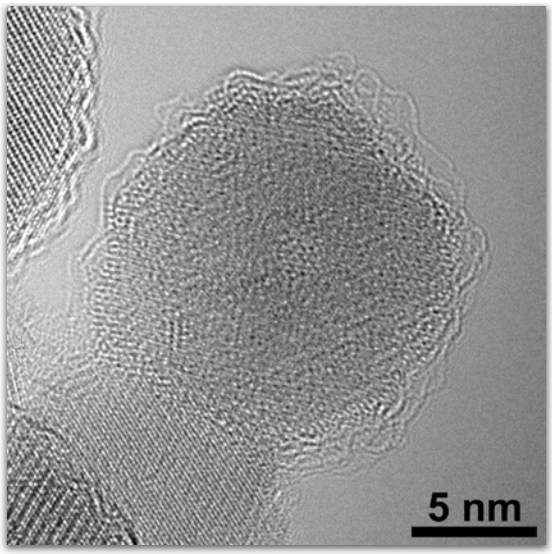

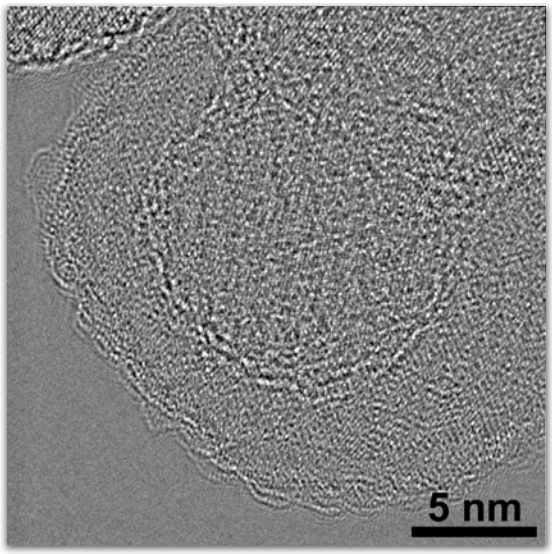

"Rainbow" mode illumination

- Use Wein filter to monochromate incident electron beam => inhomogeneous illumination with energy dispersion on one axis
- Significant reduction of energy spread; increase of temporal envelop of CTF
- See: Tiemeijer et al. Ultramicroscopy **114** (2012) 72–81

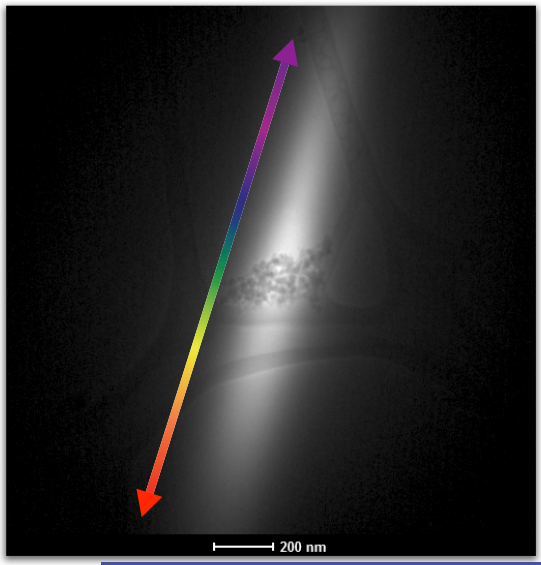

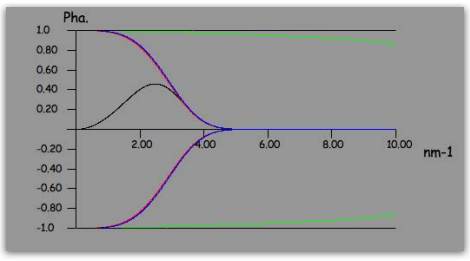

Cs: –10 µm
Cc: 1.5 mm
ΔV: 800 meV
Δf: –9.9 mm

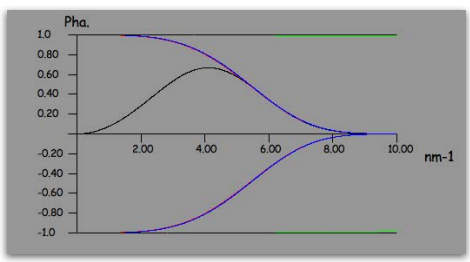

Cs: –10 µm
Cc: 1.5 mm
ΔV: 150 meV
Δf: –5.9 mm

"Rainbow" mode illumination

- Use Wein filter to monochromate incident electron beam => inhomogeneous illumination with energy dispersion on one axis
- Significant reduction of energy spread; increase of temporal envelop of CTF
- See: Tiemeijer et al. Ultramicroscopy **114** (2012) 72–81

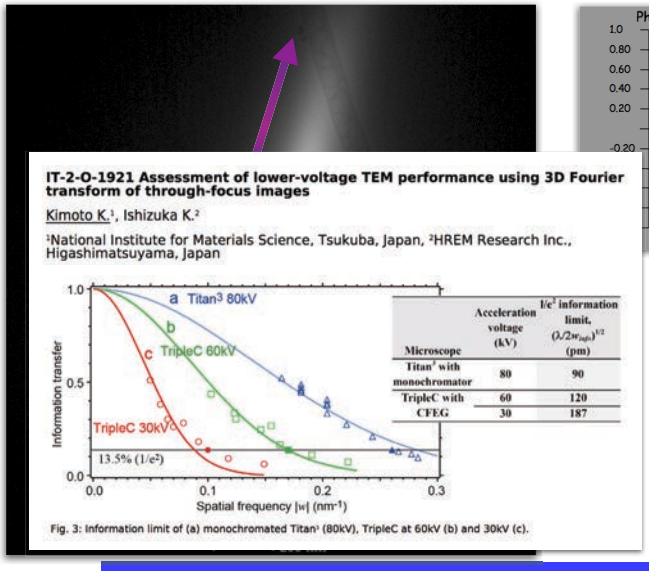

IT-2-O-1921 Assessment of lower-voltage TEM performance using 3D Fourier transform of through-focus images

Kimoto K.[1], Ishizuka K.[2]

[1]National Institute for Materials Science, Tsukuba, Japan, [2]HREM Research Inc., Higashimatsuyama, Japan

Microscope	Acceleration voltage (kV)	I/e² information limit, $(\lambda/2w_{info})^{1/2}$ (pm)
Titan² with monochromator	80	90
TripleC with CFEG	60	120
	30	187

Fig. 3: Information limit of (a) monochromated Titan³ (80kV), TripleC at 60kV (b) and 30kV (c).

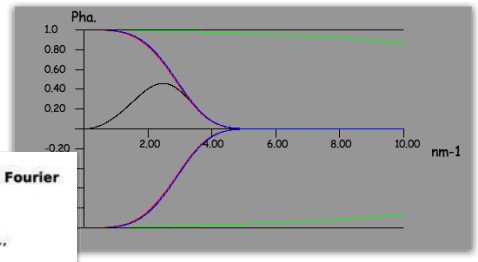

Cs: –10 µm
Cc: 1.5 mm
ΔV: 800 meV
Δf: –9.9 mm

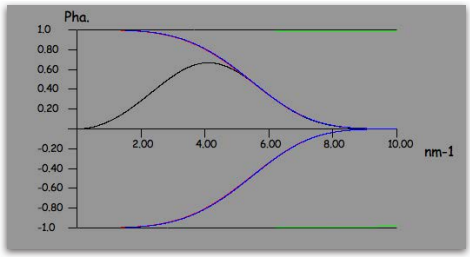

Cs: –10 µm
Cc: 1.5 mm
ΔV: 150 meV
Δf: –5.9 mm

"Rainbow" mode illumination

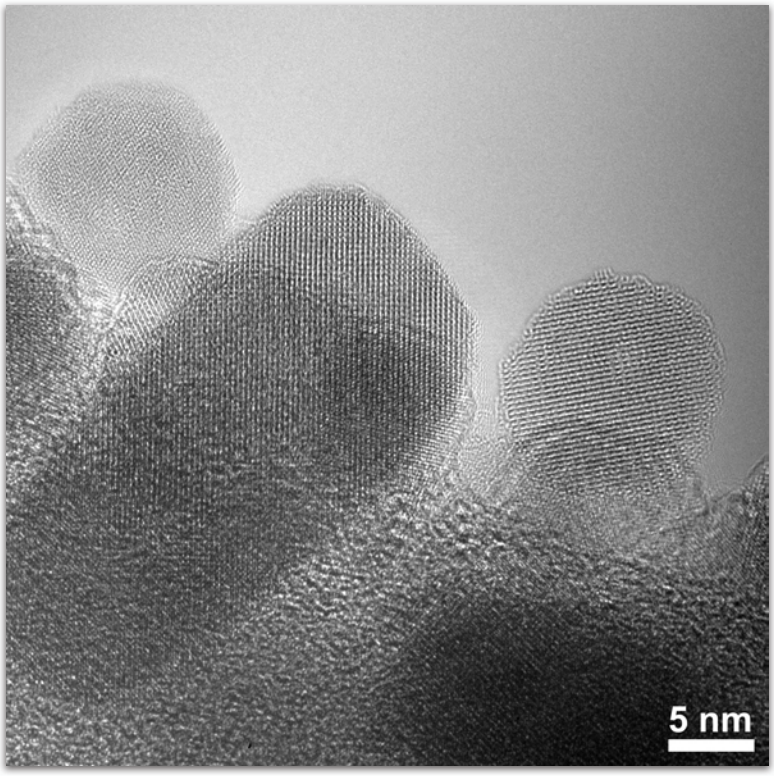

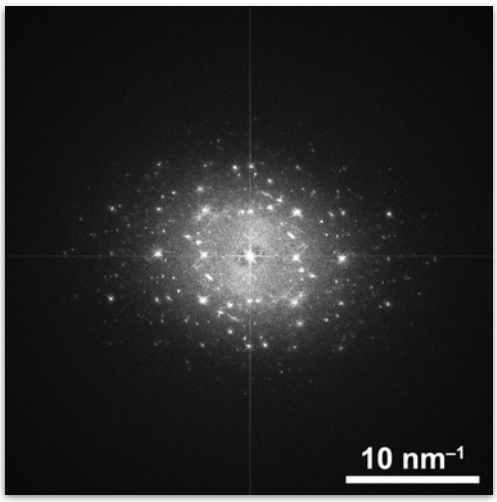

Iron oxide nanoparticles

Doped graphene, BN monolayer – Cs-STEM

Atom-by-atom structural and chemical analysis by annular dark-field electron microscopy

Ondrej L. Krivanek[1], Matthew F. Chisholm[2], Valeria Nicolosi[3], Timothy J. Pennycook[2,4], George J. Corbin[1], Niklas Dellby[1], Matthew F. Murfitt[1], Christopher S. Own[1], Zoltan S. Szilagyi[1], Mark P. Oxley[2,4], Sokrates T. Pantelides[2,4] & Stephen J. Pennycook[2,4]

- Analysis of monolayer materials: low kV essential to prevent knock-on damage; here 60 kV used (knock-on threshold for bulk graphene ~86 kV) with Nion UltraSTEM
- Medium-angle ADF (MAADF) gives intensity $I \propto Z^{1.7}$ but with increased signal intensity compared to true HAADF image. (This intensity is needed for imaging single atom by single atom; β = 58–200 mrad.) Direct atom assignment by intensity.

Krivanek et al Nature **464** (2010) 571

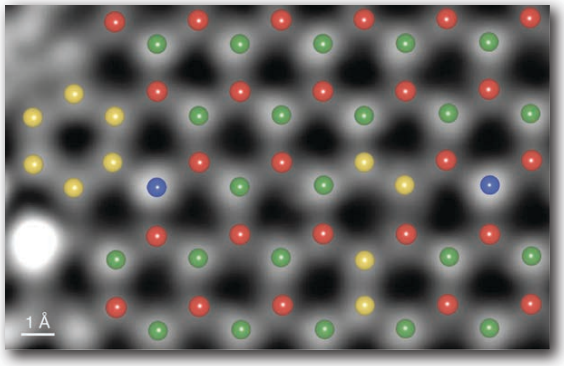

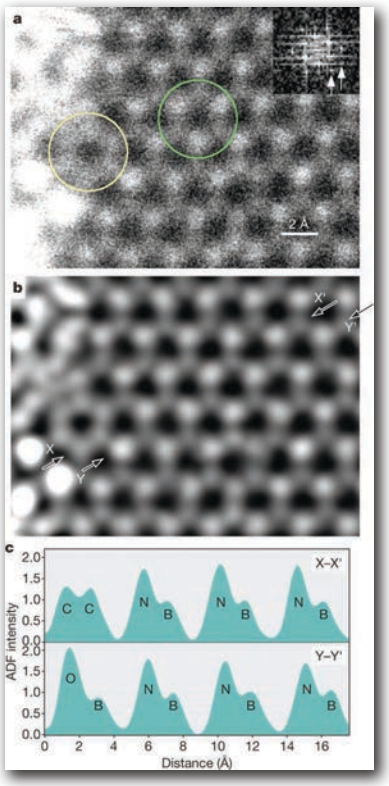

Doped graphene, BN monolayer – Cs-STEM

Experimental analysis of charge redistribution due to chemical bonding by high-resolution transmission electron microscopy

Jannik C. Meyer[1*], Simon Kurasch[1], Hye Jin Park[2], Viera Skakalova[2], Daniela Künzel[3], Axel Groß[3], Andrey Chuvilin[1,4], Gerardo Algara-Siller[1,5], Siegmar Roth[2,6], Takayuki Iwasaki[2], Ulrich Starke[2], Jurgen H. Smet[2] and Ute Kaiser[1*]

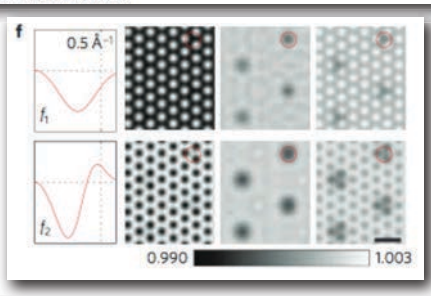

We have shown that it is possible to obtain insights into the charge distribution in nanoscale samples and non-periodic defects from HRTEM measurements. For our examples of the nitrogen substitutions in graphene and hBN layers, we can assign experimentally observed contrast features to details in the simulated electron distribution. We can detect a single light substitution atom in graphene, which is possible only because of the electronic effect. In the case of hBN, the charge redistribution leads to a loss of the elemental contrast difference. Instead, the ionic character of the material is experimentally confirmed for the single layer. One key ingredient here is the extraordinary stability of the samples under the low-voltage electron beam, which allows us to obtain extremely high signal-to-noise ratios from long exposures. The precisely defined, ultrathin sample geometry enables a straightforward analysis. The DFT-based TEM image calculation is irreplaceable for the interpretation of experimental results in these materials, and can provide insights beyond the structural configurations.

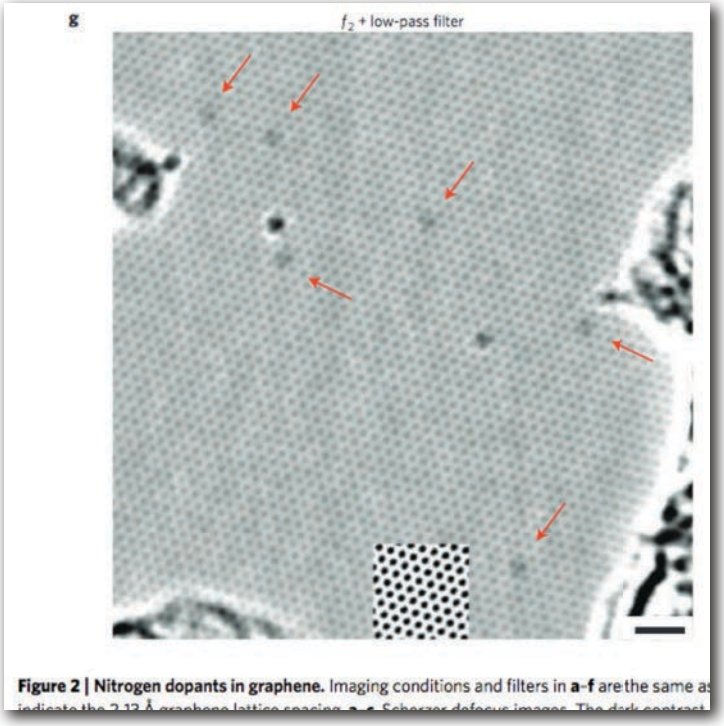

Figure 2 | Nitrogen dopants in graphene. Imaging conditions and filters in **a**–**f** are the same as

C_S-TEM of dislocations in graphene

Dislocation-Driven Deformations in Graphene

Jamie H. Warner,[1]* Elena Roxana Margine,[1] Masaki Mukai,[2] Alexander W. Robertson,[1] Feliciano Giustino,[1] Angus I. Kirkland[1]

The movement of dislocations in a crystal is the key mechanism for plastic deformation in all materials. Studies of dislocations have focused on three-dimensional materials, and there is little experimental evidence regarding the dynamics of dislocations and their impact at the atomic level on the lattice structure of graphene. We studied the dynamics of dislocation pairs in graphene, recorded with single-atom sensitivity. We examined stepwise dislocation movement along the zig-zag lattice direction mediated either by a single bond rotation or through the loss of two carbon atoms. The strain fields were determined, showing how dislocations deform graphene by elongation and compression of C-C bonds, shear, and lattice rotations.

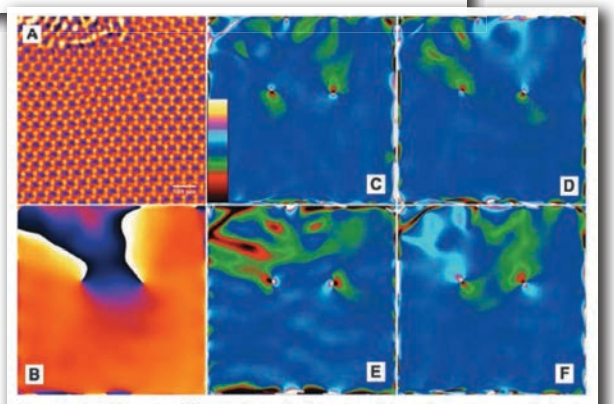

Fig. 2. Strain field mapping. **(A)** HRTEM image of a dislocation pair in graphene. GPA was applied to the HRTEM image in (A) to determine **(B)** the phase map, **(C)** ε_{xx}, **(D)** ε_{xy}, **(E)** ε_{yy}, and **(F)** rotation (in radians). The color scale for (C) to (F) is shown in (C), with a range of −0.5 (black) to +0.5 (white). For the phase map in (B), the color map is black (0) to white (2π).

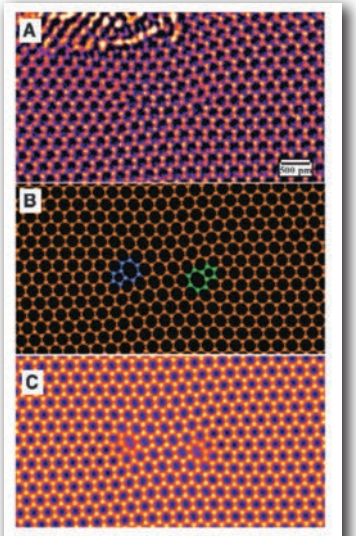

Fig. 1. Imaging edge dislocations. **(A)** HRTEM image showing two opposing (1,0) edge glide dislocations in graphene. **(B)** Structural model representing the dislocation pair (blue and green) in (A). **(C)** HRTEM image simulations using the atomic model in (B) as a supercell. False color is used for the images to aid visual inspection.

Studies of monolayer MoS_2

2010: Cs-TEM, 80 kV, TEAM 0.5 microscope

High-Resolution Microscopy DOI: 10.1002/anie.200906752

Imaging MoS_2 Nanocatalysts with Single-Atom Sensitivity**

*Christian Kisielowski, Quentin M. Ramasse, Lars P. Hansen, Michael Brorson, Anna Carlsson, Alfons M. Molenbroek, Henrik Topsøe, and Stig Helveg**

copy are provided in the Supporting Information. Figure 2 shows the experimentally restored phase of a complex exit wave function of the catalyst, and reveals a nanometer-sized particle situated on a thin graphite flake. The wave reconstruction was performed to recover all obtainable information contained in a series of 15 HRTEM images of the nanoparticle acquired at different focal points.[12] In such a phase image, the intensity maxima relate to atom positions and the contrast can reflect the chemical composition as represented in the projected scattering potential. Whilst the hexagonal shape of the nanoparticle is consistent with previously obtained images of this material,[14] the regular lattice in the interior part of the particle is now clearly visible. A lattice

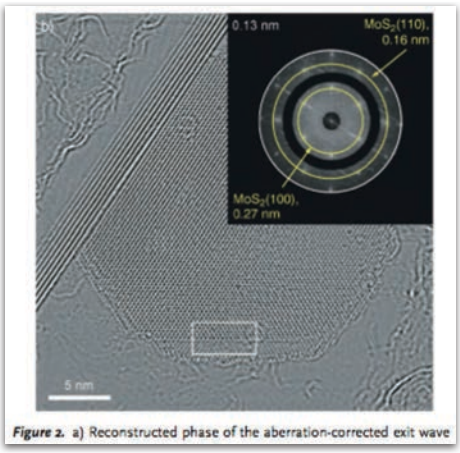

Figure 2. a) Reconstructed phase of the aberration-corrected exit wave

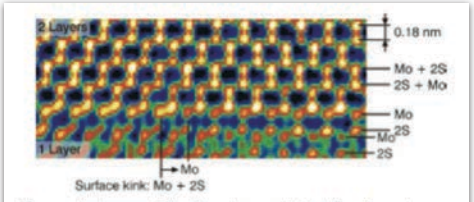

Figure 3. A close-up of the phase image obtained from the region near the bottom edge of the MoS_2 nanocrystal (partly contained in the white box of Figure 2b). A red-green-blue color scale was applied to improve readability. The upper region is assigned to a double-layer MoS_2 slab, while the lower region is a single-layer slab. More generally, the chemical composition of individual columns can unambiguously be determined. A kink from a Mo+2S column to a Mo column is indicated along the surface step from the double-layer to the single-layer MoS_2.

Studies of monolayer MoS_2

2011: Cs-STEM, 60 kV, SuperSTEM

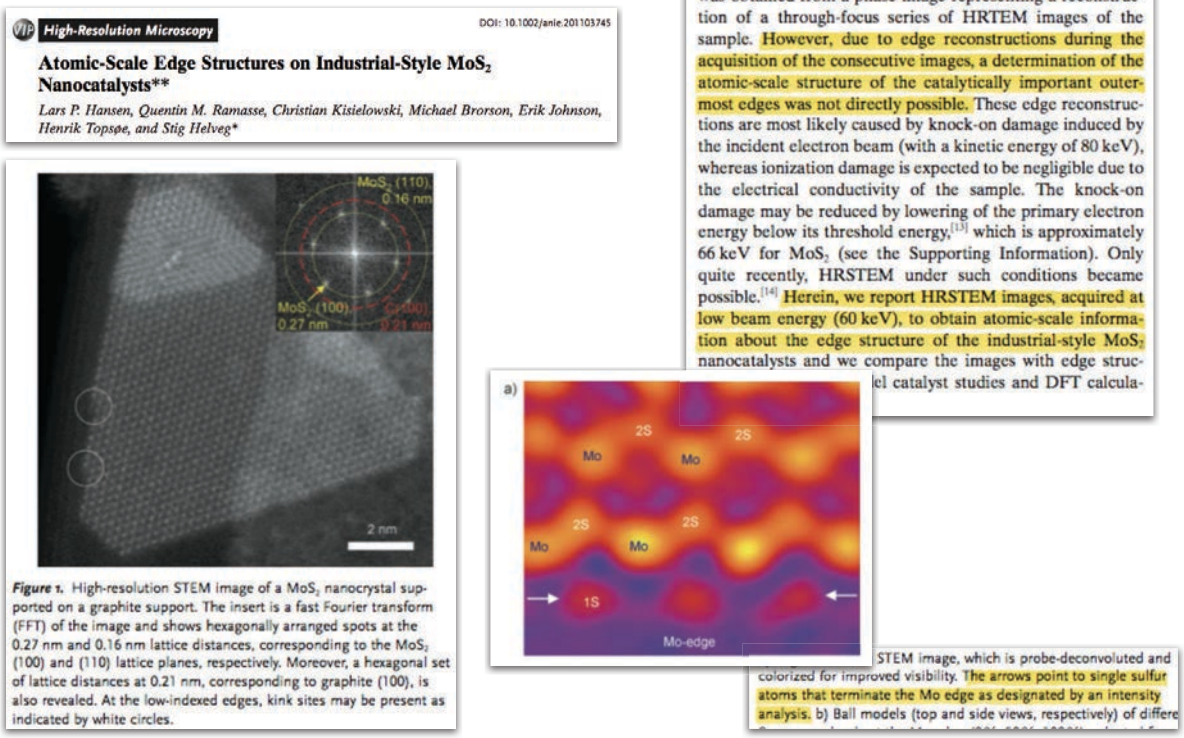

High-Resolution Microscopy

DOI: 10.1002/anie.201103745

Atomic-Scale Edge Structures on Industrial-Style MoS_2 Nanocatalysts**

*Lars P. Hansen, Quentin M. Ramasse, Christian Kisielowski, Michael Brorson, Erik Johnson, Henrik Topsøe, and Stig Helveg**

Figure 1. High-resolution STEM image of a MoS_2 nanocrystal supported on a graphite support. The insert is a fast Fourier transform (FFT) of the image and shows hexagonally arranged spots at the 0.27 nm and 0.16 nm lattice distances, corresponding to the MoS_2 (100) and (110) lattice planes, respectively. Moreover, a hexagonal set of lattice distances at 0.21 nm, corresponding to graphite (100), is also revealed. At the low-indexed edges, kink sites may be present as indicated by white circles.

indexed edge types.[12] The detailed structural information was obtained from a phase image representing a reconstruction of a through-focus series of HRTEM images of the sample. However, due to edge reconstructions during the acquisition of the consecutive images, a determination of the atomic-scale structure of the catalytically important outermost edges was not directly possible. These edge reconstructions are most likely caused by knock-on damage induced by the incident electron beam (with a kinetic energy of 80 keV), whereas ionization damage is expected to be negligible due to the electrical conductivity of the sample. The knock-on damage may be reduced by lowering of the primary electron energy below its threshold energy,[13] which is approximately 66 keV for MoS_2 (see the Supporting Information). Only quite recently, HRSTEM under such conditions became possible.[14] Herein, we report HRSTEM images, acquired at low beam energy (60 keV), to obtain atomic-scale information about the edge structure of the industrial-style MoS_2 nanocatalysts and we compare the images with edge structure model catalyst studies and DFT calcula-

STEM image, which is probe-deconvoluted and colorized for improved visibility. The arrows point to single sulfur atoms that terminate the Mo edge as designated by an intensity analysis. b) Ball models (top and side views, respectively) of differe

Titan Themis Cs-STEM: CVD monolayer MoS_2

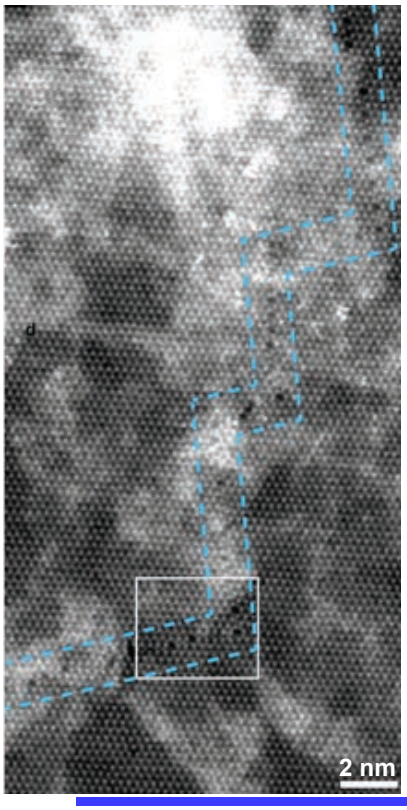

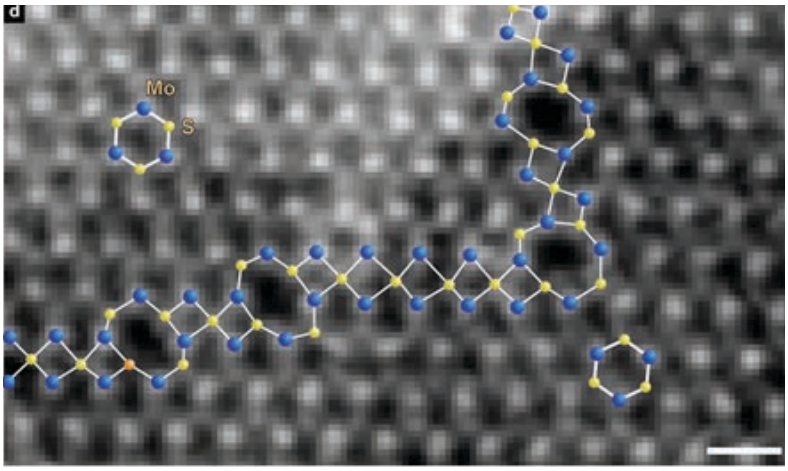

"Large-area MoS_2 grown using H_2S as the sulphur source"
Dumitru Dumcenco et al. *2D Materials* **2**(4) 2015

- 80 keV beam; even if below knock-on threshold can have beam-induced chemistry with residual gas molecules in column because not UHV (e.g. water etching).
- UHV or sample heating can be essential to good work!

Other limits

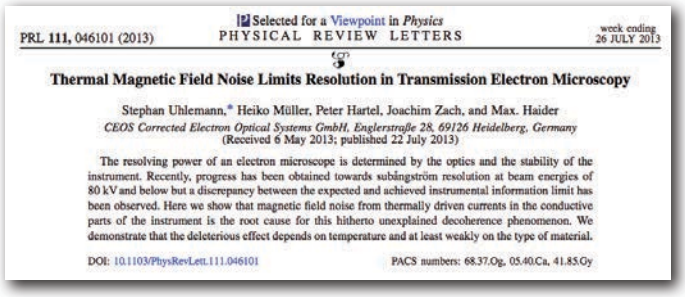

Selected for a Viewpoint in *Physics*

PRL 111, 046101 (2013) PHYSICAL REVIEW LETTERS week ending 26 JULY 2013

Thermal Magnetic Field Noise Limits Resolution in Transmission Electron Microscopy

Stephan Uhlemann,* Heiko Müller, Peter Hartel, Joachim Zach, and Max. Haider

CEOS Corrected Electron Optical Systems GmbH, Englerstraße 28, 69126 Heidelberg, Germany

(Received 6 May 2013; published 22 July 2013)

The resolving power of an electron microscope is determined by the optics and the stability of the instrument. Recently, progress has been obtained towards subångström resolution at beam energies of 80 kV and below but a discrepancy between the expected and achieved instrumental information limit has been observed. Here we show that magnetic field noise from thermally driven currents in the conductive parts of the instrument is the root cause for this hitherto unexplained decoherence phenomenon. We demonstrate that the deleterious effect depends on temperature and at least weakly on the type of material.

DOI: 10.1103/PhysRevLett.111.046101 PACS numbers: 68.37.Og, 05.40.Ca, 41.85.Gy

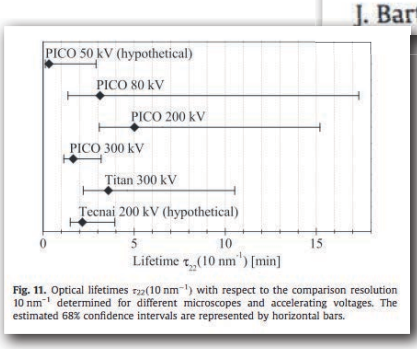

Fig. 11. Optical lifetimes τ_{22}(10 nm^{-1}) with respect to the comparison resolution 10 nm^{-1} determined for different microscopes and accelerating voltages. The estimated 68% confidence intervals are represented by horizontal bars.

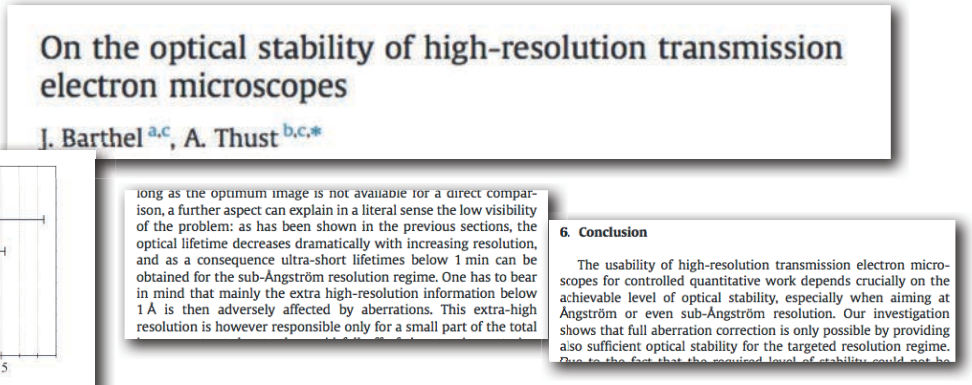

On the optical stability of high-resolution transmission electron microscopes

J. Barthel [a,c], A. Thust [b,c,*]

long as the optimum image is not available for a direct comparison, a further aspect can explain in a literal sense the low visibility of the problem: as has been shown in the previous sections, the optical lifetime decreases dramatically with increasing resolution, and as a consequence ultra-short lifetimes below 1 min can be obtained for the sub-Ångström resolution regime. One has to bear in mind that mainly the extra high-resolution information below 1 Å is then adversely affected by aberrations. This extra-high resolution is however responsible only for a small part of the total

6. Conclusion

The usability of high-resolution transmission electron microscopes for controlled quantitative work depends crucially on the achievable level of optical stability, especially when aiming at Ångström or even sub-Ångström resolution. Our investigation shows that full aberration correction is only possible by providing also sufficient optical stability for the targeted resolution regime.

J. Barthel, A. Thust / Ultramicroscopy 134 (2013) 6–17

C_S-TEM

- Harder to align precisely on zone axis (need to flip from diffraction to image)
- Interpret via: focal series reconstruction; negative Cs imaging; simulation
- Easy to obtain fringe image but precise Scherzer focus potentially challenging
- Contrast inversions with thickness remain; but can image very thick samples
- Damage: beam intensity spread, but total dose may be higher
- Coherent imaging: CTF determines resolution limit
- Atomic column analytics with (C_C-corrected) EFTEM less proven
- Camera properties important (MTF, "Stobbs factor")
- Picometer measurement precision
- Dynamics studies 25 fps easy, 1000 fps now possible (good for ETEM)
- Can still image samples which contaminate, e.g. organic molecules

C_S-STEM

- Easier to align precisely on zone axis (always in diffraction mode)
- Interpret via HAADF/MAADF/BF/ABF/ iDPC image
- Very limited DOF but very precise focus; camera-like focus
- Arguably thickness insensitive: sample first nms of thickness
- Damage: strong local intensity, but total dose may be lower
- Incoherent imaging: OTF determines resolution limit for HAADF
- Atomic column analytics with STEM-EELS; STEM-EDX also works
- Scan instabilities and detector noise important; need very stable scan
- Equally good precision
- Slower, but possible to follow movement of single atoms
- Need contamination-free samples only UHV possibility